Neutron transmutation doped far-infrared p- Ge laser

E. W. Nelson, M. V. Dolguikh, A. V. Muravjov, E. S. Flitsiyan, T. W. Du Bosq, R. E. Peale, S. H. Kleckley, C. J. Fredricksen, and W. G. Vernetson

Journal of Applied Physics is pleased to announce André Anders as its new Editor-in-Chief

Neutron transmutation doped far-infrared *p*-Ge laser

E. W. Nelson, M. V. Dolguikh, A. V. Muravjov,[a] E. S. Flitsiyan, T. W. Du Bosq, and R. E. Peale[b]
Department of Physics, University of Central Florida, Orlando, Florida 32816

S. H. Kleckley and C. J. Fredricksen
Zaubertek, Inc. 1809 E. Broadway St. #313 Oviedo, Florida 32765

W. G. Vernetson
Department of Nuclear and Radiological Engineering, University of Florida, Gainesville, Florida 32611

A far-infrared *p*-type germanium laser with active crystal prepared from ultra pure single-crystal Ge by neutron transmutation doping (NTD) is demonstrated. Calculations show that the high uniformity of Ga acceptor distribution achieved by NTD significantly improves average gain. The stronger ionized impurity scattering due to high compensation in NTD Ge is shown to have insignificant negative impact on the gain at the moderate doping concentrations sufficient for laser operation. Experimentally, this first NTD laser is found to have lower current-density lasing threshold than the best of a number of melt-doped laser crystals studied for comparison.   © *2004 American Institute of Physics.*   [DOI: 10.1063/1.1753659]

INTRODUCTION

Far-infrared laser emission from hot holes in *p*-Ge, has been intensely investigated.[1] The mechanism is direct optical transitions between light- and heavy-hole valence subbands at liquid-helium temperatures in crossed electric and magnetic fields. Population inversion is created for certain ratios of electric and magnetic fields. Light holes accumulate in relatively long-lived closed cyclotron orbits, while heavy holes are quickly scattered by optical phonons. Each scattered hole has a finite probability to be scattered to the light-hole subband, which builds a population inversion between subbands. The resulting broad gain spectrum on intersubband transitions allows picosecond far-infrared output pulses[2–8] or allows broad tunability with high spectral density over the 1.5 to 4.2 THz (50 to 140 cm^{-1}) frequency range (70 to 200 μm free-space wavelengths).[9–14]

The traditional pumping scheme for bulk active *p*-Ge crystals is thermally limited to low duty cycles. A burst of optical phonons is generated for each generated far-infrared photon, such that the physical limit of the pumping efficiency is less than 1%, and the active crystal quickly overheats. The resulting increase in lattice absorption and decrease in light hole lifetime terminate the laser emission. With a maximum working temperature around 20 K, the emission pulse lasts less than 10 μs for ~1 cm^3 active volume and ~1 W output power. The cooling rate in liquid helium of less than 10 W/cm^2 limits the repetition rate to ~100 Hz. In principle, continuous operation could be achieved by reducing the active volume below 1 mm^3,[15] but

this increases cavity losses, which for a typical gain of only ~0.01–0.1 cm^{-1} is a critical disadvantage.

To overcome the thermal limitations, it is desirable in *p*-Ge lasers to achieve the highest possible gain. Effort has been devoted to determine the factors responsible for the gain. Active crystal geometry,[16] crystallographic orientation,[17,18] doping concentrations,[1] deep acceptor doping,[19] uniaxial stress,[20–22] and optimization of electrodynamic cavities[23] have been studied. Even moderate improvement of the gain would allow reduced active crystal volume and thus reduced power dissipation and improved cooling efficiency. Still, measured values of gain ranging from[24] 0.01 to[25] 0.1 cm^{-1} fall short of recent predictions,[2,26] which suggest the possibility of gain as large as 0.4 cm^{-1} for certain photon wavelengths, applied field strengths, and orientations.

A probable cause of the observed low gain is field inhomogeneity within the active crystal. It is known that a deviation from perpendicularity of applied $\mathbf{E} \times \mathbf{B}$ fields by only 1° causes a remarkable reduction of gain.[1] A component of $\mathbf{E}$ parallel to $\mathbf{B}$ (Fig. 1, lower inset) accelerates trapped light holes in the direction of $\mathbf{B}$ until they scatter on optical phonons, decreasing the light-hole lifetime and therefore gain. Hence, field nonuniformity would allow gain as high as the theoretical limit to exist only locally, with losses that must be overcome elsewhere in the medium, giving low values for the observed average gain.

The magnetic field, usually created by a superconducting solenoid or permanent-magnet assembly,[27] is quite uniform within the active crystal. However, $\mathbf{E}$-field uniformity is degraded under nonlinear conduction conditions by space and surface charge, which appear due to the Hall effect, anisotropic conductivity, and nonuniform doping. Proper choice of orientation for the active crystal eliminates those $\mathbf{E}$ components along $\mathbf{B}$ caused by the Hall effect and anisotropy, but

---

[a] On leave from Institute of the Physics of Microstructures, RAS, Nizhny Novgorod, Russia.

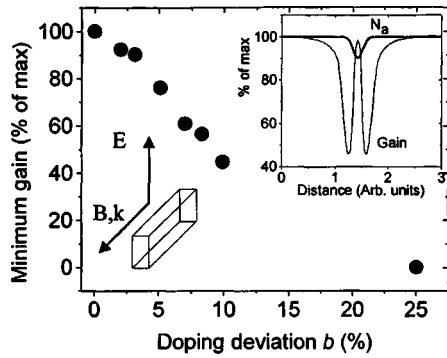[b] Author to whom all correspondence should be addressed; electronic mail: rep@physics.ucf.edu

FIG. 1. Lower inset: Schematic of p-Ge laser crystal with orientation of applied fields ($\mathbf{E}$, $\mathbf{B}$) and direction of laser output ($\mathbf{k}$). Upper inset: Doping and gain profiles. Symbols: Simulation of peak local gain reduction at 100 cm^{-1} as a function of doping-anomaly scale.

nonuniform spatial distribution of acceptors is uncontrollable in a given laser rod.

Active p-Ge laser crystals are traditionally Ga-doped during melt growth. Room temperature resistivity variations typically exceed 4%–10% over both macroscopic (centimeter) and microscopic (sub-millimeter) length scales.[28] In the lightly doped (35 to 40 Ω cm) material required for p-Ge lasers, intrinsic carriers significantly contribute to the room temperature resistivity. Hence, variations in acceptor concentration can greatly exceed room-temperature resistivity variations.

This article presents results of neutron transmutation doping (NTD)[28–30] to produce uniformly doped p-Ge laser material. Some preliminary results have been reported in Refs. 31 and 32. Room temperature resistivity variations of NTD Ge over submillimeters to centimeters lengths are less than 0.7%.[28] The NTD method immerses undoped Ge in the homogeneous neutron flux of a nuclear reactor. Three of the five stable natural Ge isotopes, ^{70}Ge, ^{74}Ge, and ^{76}Ge are transmuted by thermal neutrons into ^{71}Ga (shallow acceptor), ^{75}As (shallow donor), and ^{77}Se (double donor), respectively. The remaining two isotopes Ge^{72} and Ge^{73}, transmute into other stable Ge isotopes Ge^{73} and Ge^{74}, respectively. The low doping levels needed for p-Ge lasers require less than 1 h irradiation in a typical reactor. The donors As and Se are produced in lower concentrations than the acceptor Ga, so that NTD Ge is p-type with reported compensations $K = N_d/N_a$ in the range 0.32–0.40,[29,30] where $N_{d(a)}$ is the concentration of donors (acceptors). In the few melt-doped p-Ge lasers tested for compensation, the value has been between[33] 0.07 and[34] 0.3, but the maximum allowable compensation for a p-Ge laser is uncertain.

A practical consideration in favor of the NTD process for producing p-Ge lasers is that the ultra-pure starting material is readily available from commercial suppliers. Large single crystals of this highly refined germanium are used in gamma-ray detectors. In contrast, suitable melt-doped p-Ge is not a standard item of commerce.

Long lived radioactivity can be generated in natural germanium only by activation of impurities, since final transmutation products of natural Ge isotopes are stable and result from rapid decays. Most of the expected impurities in ultra-pure Ge starting material generate isotopes with half-lives from seconds to minutes. Preirradiation polishing with diamond ensures that residual surface impurities are mainly carbon. Diamond powder may contain Zn as a (removable) impurity, which can lead to radioactive Zn-65. Cleaning of cut laser rods in HF vapor removes surface contamination without introducing metal ions.

THEORETICAL CONSIDERATIONS

It is important to emphasize that, due to saturation of the current in the strong applied $\mathbf{E}$-fields required for lasing, even moderate doping inhomogeneity dramatically disrupts the $\mathbf{E}$-field homogeneity within the active sample. This drastically reduces the gain because of its strong sensitivity to deviation in angle between local-$\mathbf{E}$ and applied-$\mathbf{B}$ fields from 90°. To obtain quantitative estimates of this effect, the internal $\mathbf{E}$-field distribution was found by numerically solving the equation

$$\mathrm{div}(\mathbf{J}) = 0 \qquad (1)$$

in the presence of a doping anomaly using the finite element method, where $\mathbf{J}$ is the current density. A simple ad hoc model of the nonohmic current in the near-saturation regime that qualitatively gives the correct dependence is

$$\mathbf{J} = \sigma \mathbf{E}^{(1-s)}, \qquad (2)$$

with saturation factor $s = 0.75$. Effects of the $\mathbf{B}$-field on current redistribution were neglected. A doping anomaly of the form

$$N_a/N_{a0} = 1 - b\,\mathrm{Exp}[-r^2/R^2] \qquad (3)$$

was assumed, where N_a is the acceptor concentration, b is the anomaly magnitude, and R its direction-dependent length scale. The calculated $\mathbf{E}$-field redistribution was combined with gain versus $\mathbf{E}$-field-deviation results from Monte-Carlo simulation[26] to determine the spatial gain distribution near the anomaly.

The upper insert in Fig. 1 shows acceptor concentration and gain profiles for a spherical doping anomaly. The gain dependence is plotted for a profile oriented at 45° to the applied $\mathbf{E}$-field, which corresponds to the strongest gain distortion. The calculations showed that distorting the anomaly from spherical shape distorts the gain profile, but the maximum gain reduction stays approximately the same and depends mainly on the degree of the anomaly b. The dependence of the minimal gain versus b is plotted as symbols in Fig. 1. These results are valid for any anomaly scale starting from light hole mean free path (10 μm) to the full size of the active crystal.

Although the *average* gain reduction will depend on the individual pattern of the acceptor distribution, the Fig. 1 dependence characterizes the effect of non-uniform doping. The region with degraded gain always has much larger spatial extent than the doping anomaly. For melt-doped p-Ge with just 15% doping inhomogeneity, the gain in certain regions drops threefold. These considerations can explain the observed performance variations for different crystals cut from the same melt-doped boule, which will be demonstrated below.
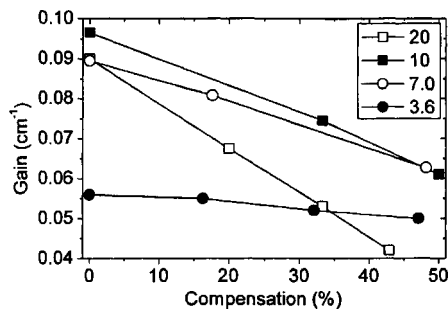
FIG. 2. Monte Carlo calculation of gain at 100 cm^{-1} vs compensation for different hole concentrations. The legend gives hole concentrations in units of 10^{13} cm^{-3}. Simulation parameters were $E = 1.25$ kV/cm, $B = 1$ T, and $T = 10$ K.
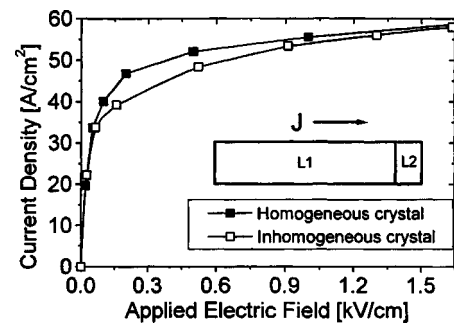

FIG. 3. Monte Carlo calculation of current density as a function of applied electric field for a homogeneous and an inhomogeneous crystal. Inhomogeneity distribution and direction of current are shown schematically in the inset. The total impurity concentration was taken to be $N_i = 6.7 * 10^{13}$ cm^{-3} with 30% compensation ($p = N_a - N_d \sim 3.6 \times 10^{13}$ cm^{-3}).

Monte Carlo simulation[26] provides predictions for the effect of compensation on gain. Simulation results are presented in Fig. 2, where gain at 100 cm^{-1} is plotted versus compensation for four different hole concentrations. (These Monte Carlo calculations differ from Ref. 2 by assuming isotropic dispersion and implementing a more accurate approach to impurity and electron–electron scattering.[26] Thus the gain values in Fig. 2 are smaller than those found in Ref. 2, where a maximum gain of 0.4 cm^{-1} was calculated.) At zero compensation, the hole concentration that maximizes the gain is 10^{14} cm^{-3}, which is close to the experimental value of $\sim 7 \times 10^{13}$ cm^{-3}.[1] The effect of compensation is in all cases to lower the gain, but this effect becomes less and less pronounced with decreasing hole concentration. At the concentration 3.6×10^{13} cm^{-3}, the effect of compensation is almost negligible.

Hole concentration p may be determined from room temperature resistivity ρ of germanium samples according to

$$1/\rho = e(\mu_p p + \mu_n n_i^2/p) \qquad (4)$$

where e is the elementary charge, and $\mu_{n,p}$ are room temperature mobilities of electrons and holes, taken as 3900 and 1900 cm^2/V*s, respectively.[35] The value for intrinsic carrier concentration $n_i = 1.87 \times 10^{13}$ cm^{-3} at 23 °C sample temperature according to Ref. 36. A complementary measure of p may be deduced from the low temperature saturated current density according to

$$J_s = e v_s p, \qquad (5)$$

where v_s is the average saturated hot hole velocity in Ge at liquid helium temperature. A value of $v_s = 0.98 \times 10^5$ m/s was determined by Monte Carlo simulation with applied fields $E = 1$ kV/cm and $B = 0$. Compensation K is related to p and N_a by

$$p = (N_a - N_d) = N_a(1 - K). \qquad (6)$$

An indication of doping homogeneity is saturation current behavior at high electric field, where the dominant scattering mechanism is optical phonon scattering. Simulated saturation curves (Monte Carlo method[26]) are presented in Fig. 3 for homogeneous and inhomogeneous crystals. The latter is a rather extreme case, where the crystal length L is divided into two sections, one of length $0.9L$ and concentration p, and one with length $0.1L$ and concentration $0.7p$. The

inhomogeneous curve was obtained using the average carrier velocity versus electric field, obtained from the Monte Carlo simulation in the homogeneous case, together with the continuity condition for current. The transition between ohmic and saturated regions is sharper for the homogeneous crystal.

EXPERIMENTAL DETAILS

To determine the statistical dispersion of laser performance resulting from random doping anomalies, 18 laser rods were prepared from Ge melt-doped with Ga, designated material C. The original boule was 9.9 cm in length with 3.4 cm diameter. The vendor (Tydex, St. Petersburg, Russia) specified the axial orientation as [110], the range of resistivity as 34 to 46 Ω cm, and the dislocation density as 1000 cm^{-2}. The radial crystallographic orientations were determined by HeNe laser light scattering from suitably etched surfaces.[37] The boule was cross cut into two cylinders of length 46.4 and 52.4 mm using a wire saw. These cylinders were then cut in half longitudinally. A low-speed diamond saw then cut the longer hemi-cylinder into nine laser rods (C1–C9), as shown in Fig. 4. Nine more laser rods (C10–C18) were cut from the shorter hemicylinder. Table I lists dimensions of the laser rods studied.

Laser cavities were formed using SrTiO$_3$ mirrors attached to the active sample end faces. The back mirror covered one face of the active crystal. The output mirror on the opposite face was of a smaller area to allow radiation to escape around the mirror edge. E-field pulses of 1–2 μs duration were generated in the laser crystal by applying high voltage with a thyratron pulser to ohmic contacts on lateral surfaces of the crystal. Current through the active crystal was monitored using a fast current probe (Pearson 411). The magnetic field was supplied by a superconducting solenoid in Faraday configuration. Laser emission was detected using a Ge:Ga photoconductor immersed in liquid helium at 4 K in the same dewar.

For neutron transmutation doping, a rod measuring $\sim$37 $\times 6 \times 5$ mm^3 was cut from high purity germanium (Perkin Elmer). The electrically active impurity concentration was specified as 1.02×10^{11} cm^{-3}. Neutral impurities (Si,H,O,...,) may be present in higher concentrations. The rod was rinsed in spectroscopy-grade acetone, etched in HF vapor, and fi-
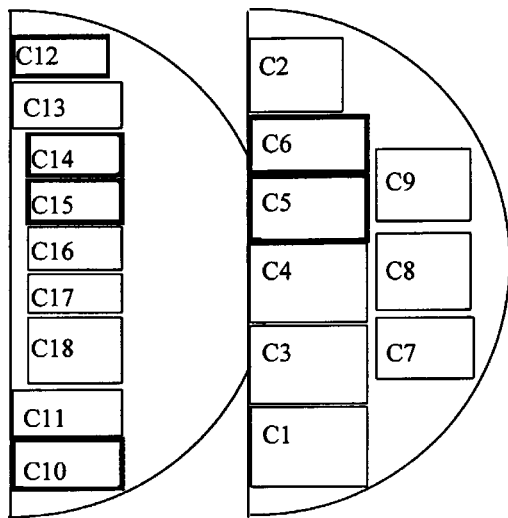
FIG. 4. Crystals cut from a commercial *p*-Ge boule of melt-doped material C. The crystal cross sections are shown to scale and labeled with their Table I designations. The six best performers (lowest **E**-field thresholds) are highlighted.

nally rinsed in distilled water to remove trace surface contaminants. The rod was wrapped in polyethylene and irradiated in the central vertical port of the University of Florida Training Reactor (Gainesville, Florida) (UFTR, 1.5 $\times 10^{12}$ n/cm^2 s thermal neutron flux) for 25 min (becoming material D). Additional fast neutron flux gave an estimated effective thermal neutron flux for the intended reactions of 3×10^{12} n/cm^2 s. After irradiation, radionuclides present in the rods were identified using a high purity germanium detection system. Total emission rate was determined with a Geiger counter (Ludlum-3). Seven days after irradiation at UFTR, the radionuclides detected by γ-emission spectroscopy in material D were primarily Ge-77, Ge-75, and As-77.

TABLE I. Laser rods. Material C is melt doped. Material D is neutron transmutation doped. An asterisk (*) designates nonworking lasers. The dimensions given are the long axis (**B**-field direction), **E**-field direction, and direction perpendicular to **E**, respectively. Crystallographic orientations are [110]$\times$[$-$110]$\times$[001] for these directions for all crystals.

Designation	Dimensions [mm^3]	**E**-field lasing threshold (kV/cm)
C1	51.8$\times$7.6$\times$5.1	0.78
C2	51.2$\times$7.5$\times$5.2	0.91
C3	51.8$\times$7.6$\times$5.1	1.1
C4	51.3$\times$7.5$\times$5.1	1.0
C5	51.2$\times$7.6$\times$4.2	0.72
C6	51.2$\times$7.6$\times$3.65	0.64
C7	51.2$\times$6.35$\times$4.0	0.78
C8	51.8$\times$6.1$\times$5.0	0.90
C9	51.8$\times$6.05$\times$4.75	1.3
C10	45.45$\times$7.0$\times$3.2	0.86
C11	45.45$\times$6.95$\times$3.1	0.86
C12	45.45$\times$6.0$\times$2.5	0.72
* C13	45.45$\times$6.9$\times$3.1	—
C14	45.7$\times$5.9$\times$2.6	0.64
C15	45.7$\times$6.0$\times$2.5	0.67
C16	45.7$\times$6.1$\times$2.85	0.82
C17	45.7$\times$5.9$\times$2.51	0.93
* C18	45.7$\times$5.9$\times$4.3	—
D1	17.40$\times$6.16$\times$2.44	0.71

Thirteen days after irradiation, only As-77 was detectable. At that time, the germanium was found to emit $\sim$0.01 mR/hr, which is indistinguishable from background.

The NTD rods were tested for laser action before and after annealing. For initial laser testing, the NTD sample measured approximately $37 \times 6 \times 5$ mm^3. This crystal was then cut into four parts measuring $18.38 \times 6.16 \times 2.44$ mm^3 and tested again for lasing prior to annealing. One of these crystals (D1) was annealed 30 min at 390 °C, repolished, and tested for laser emission. Table I gives its final dimensions.

To obtain information on gallium concentration and compensation, neutron activation analysis (NAA) was performed on samples of materials C and D. Typical sample mass was between 0.1–0.3 g. Samples were placed into 0.3-ml polypropylene vials and irradiated for 30 min at Uzbekistan Academy of Science (Tashkent, Uzbekistan) reactor (10 kW, open pool, 3×10^{13} thermal neutron/cm^2*s). Neutron capture by the ^{71}Ga (which exists in both NTD and melt-doped *p*-Ge) produces the isotope ^{72}Ga ($T_{1/2}$ = 14.1 h), whose 834 keV γ-line is the Ga signature used for the NAA. After a six-day cooling-off period, which allows the majority of the interfering isotope ^{69}Ge to decay, a Ge:Li detector counted the γ-ray emission. Relative ^{71}Ga concentration was determined from the ^{72}Ga 834 keV line strength. In NTD samples, the isotopic abundance of ^{71}Ga is 100%, but the natural abundance of ^{71}Ga in the melt-doped samples is only 39.89%. Therefore, the 834 keV line strength for melt-doped samples was multiplied by the factor 1/0.3989.

For resistivity measurements, a constant current ($<$15 mA to avoid heating) was applied, and resistance was determined from the measured potential drop. Resistivity was calculated from these data using rod dimensions. Hole concentration p was then found from Eq. (4). Values for p were also determined from the saturated current density according to Eq. (5). Comparison of p versus gallium concentration from neutron activation analysis then provides information about compensation K, according to Eq. (6).

To compare the shape of current saturation curves, two identically shaped rods of materials C and D were immersed in liquid helium and subjected to microsecond current pulses along their long axis [110]. The experiments were performed in the presence of a small magnetic field (0.19 T) applied axially.

RESULTS

Laser generation zones in the space of applied E and B fields for melt-doped samples C1–C12 and C14–C17 are presented in Fig. 5. Samples C13 and C18 failed repeatedly to produce laser emission, while all other C crystals worked during their first trials. A large variation in electric field threshold is observed. Crystal C6 has the lowest electric field and current density thresholds. The latter has the value 74.4 A/cm^2 for C6.

Far-infrared laser emission from NTD laser crystal D1 was observed only after annealing. The region of observed laser emission in the space of applied electric and magnetic fields is plotted in Fig. 5. The electric field threshold is comparable to the lowest thresholds found in melt-doped mate-
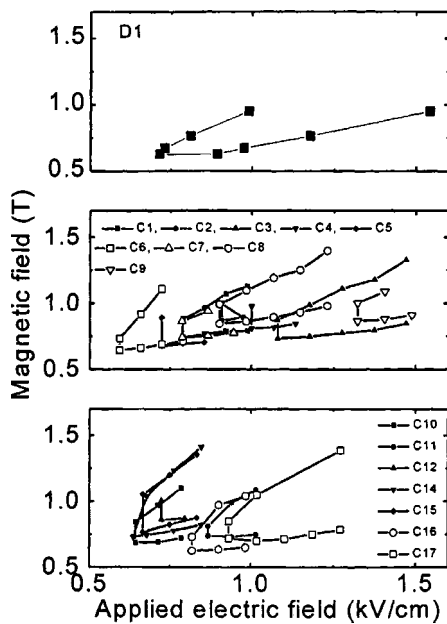
FIG. 5. (top) Zone for observed far infrared laser emission for annealed NTD laser rod D1 in applied field space. (middle) Laser generation zones of C1–C9 and (bottom) C10–C17.

rial C, but the current density threshold is considerably lower at 50.7 A/cm^2.

Saturated current density versus electric field applied via lateral laser contacts was measured for D1 and C6 in liquid helium. For a given crystal, saturation curves for different applied magnetic fields asymptotically approach the same saturated current density J_s. Using Eq. (5), hole concentrations p are determined from J_s values and plotted against normalized gallium concentration from NAA as open symbols in Fig. 6. Values of p determined from resistivity data and Eq. (4) are plotted as solid symbols in Fig. 6. The crystal D1 has a lower hole concentration than C6 by a factor 1.04 (resistivity data) to 1.5 (current saturation data). Since the Ga concentration of D1 is higher, its compensation is higher. By calibrating the concentration scale using p, the expected compensation of 32%–40% for D1, and Eq. (6), lines of zero
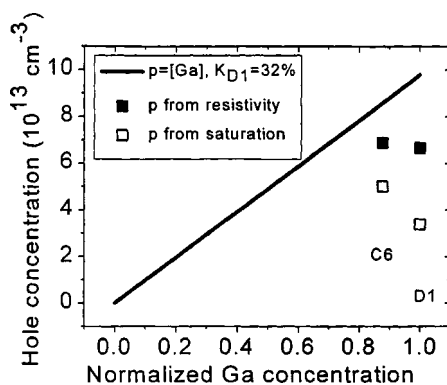

FIG. 6. Hole concentration p as a function of normalized Ga concentration for melt-doped crystal C6 and for annealed NTD crystal D1 as determined by room temperature resistivity (solid symbols) and as determined by saturation current density at 4 K (open symbols). The zero compensation line is found by calibrating the normalized concentration using the D1 p value from resistivity and assuming 32% compensation.
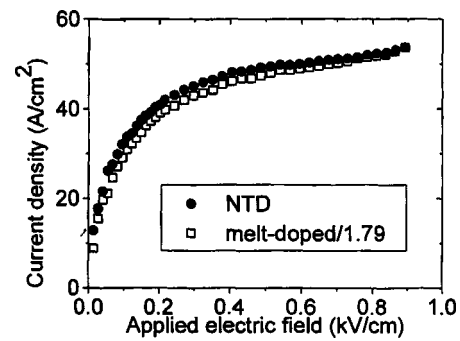

FIG. 7. Current density vs applied electric field for annealed NTD (D) and melt-doped (C) p-Ge crystals of identical dimensions. A small longitudinal magnetic field of 0.19 T is applied to suppress electron injection. Sample temperature was 4 K. The data are scaled to have the same maximum value. The scaling factor is given in the legend.

compensation (or $p=[Ga]$) can be drawn. The straight line in Fig. 6 is the $K=0$ line found using the p values from resistivity data and a K value of 32% for D1. This suggests that the compensation of the C6 crystal is ~20%. If K was set to 40% for D1, the compensation of C6 would be ~30%. Hence, the NTD laser crystal has compensation 1.3 to 1.6 times higher than the best of the melt-doped crystals studied.

Current saturation curves were compared for rods of material C and annealed (1 h at 390 °C) material D having identical geometry and axial current flow (Fig. 7). The transition to saturation is slightly sharper for the NTD crystal than for the melt-doped crystal. The difference is less than the simulated Fig. 4 curves, though it was expected that real crystals would have less extreme inhomogeneity than the simulation model used for Fig. 4. Nevertheless, these data support the assertion that the doping uniformity achieved in the NTD crystal is higher than in the melt-doped crystal studied.

DISCUSSION

Electric field threshold of the laser operation is a qualitative indicator of laser gain. Thus, Fig. 5 indicates a large variation in the quality of laser rods prepared from the same melt-doped boule and tested under identical conditions. This variability can be attributed to the poor uniformity of low-concentration doping for melt-doped crystals. Since most of the best performing crystals tend to come from the same portion of each hemicylinder (Fig. 3), there is likely substantial doping inhomogeneity over centimeter length scales. Hence, a typical melt-doped p-Ge boule will have low yield of good laser rods.

Current density threshold for D1 is a factor 1.5 times smaller than that found for the best of the C crystals (C6). This positive result occurs despite a much smaller active volume for D1. The larger number of round trips required to build up laser oscillation therefore implies that the low D1 threshold occurs despite higher output coupling, mirror loss, and other potential electrodynamic losses.

The NTD p-Ge laser material was found to be a factor 1.3 to 1.6 times more highly compensated than the best of the melt-doped crystals studied for comparison. Nevertheless, the current density threshold for lasing was found to be

considerably lower in the NTD crystal. This observation is consistent with the prediction from Monte Carlo calculations (Fig. 2) that compensation has little negative effect at hole concentration 3.6×10^{13} cm^{-3} (the value for the NTD laser crystal tested.)

A controllable, repeatable process such as NTD should allow higher yield of good laser rods per kg of material. Given current prices for melt-doped ($\sim$\$3/g) and ultra-high purity Ge crystals ($\sim$\$5/g), the yield need only be twice better to make NTD economically preferable. The neutron-irradiation fee at UFTR is \$100/h, which is negligible compared with other costs of producing a commercial p-Ge laser (primarily cryogenics and specialized electronics). Residual radiation is equivalent to background, so properly aged NTD Ge poses no health risk. High-purity Ge starting material for NTD is commercially available while suitable melt-doped Ge is not a standard commercial item.

SUMMARY AND CONCLUSIONS

A far-infrared p-Ge laser with neutron transmutation doped active crystal was demonstrated. A high degree of uniformity for the Ga-acceptor distribution, easily obtained by NTD, but unusual in melt-doped Ge, was shown to be important for p-Ge laser operation. Current saturation behavior supports the expected higher homogeneity for this doping process. Despite the negative factor of higher compensation, this first unoptimized NTD p-Ge laser achieves a current density threshold significantly smaller than the best of 18 melt-doped lasers studied for comparison. Optimization of the NTD process should eventually permit smaller rods with lower thresholds, increased gain, and higher duty cycles.

ACKNOWLEDGMENTS

[1] E. Bründermann, in *Long-Wavelength Infrared Semiconductor Lasers*, edited by H. Choi (Wiley, New York, 2004), p. 279.
[2] R. C. Strijbos, J. G. S. Lok, and W. T. Wenckebach, J. Phys.: Condens. Matter **6**, 7461 (1994).
[3] J. N. Hovenier, A. V. Muravjov, S. G. Pavlov, V. N. Shastin, R. C. Strijbos, and W. Th. Wenckebach, Appl. Phys. Lett. **71**, 443 (1997).
[4] A. V. Muravjov, R. C. Strijbos, C. J. Fredricksen, H. Weidner, W. Trimble, A. Jamison, S. G. Pavlov, N. Shastin, and R. E. Peale, in *Radiative Processes and Dephasing in Semiconductors*, edited by D. S. Citrin (Optical Society of America, Washington, DC 1998) OSA-TOPS **18**, 102 (1998).
[5] J. N. Hovenier, T. O. Klaassen, W. Th. Wenckebach, A. V. Muravjov, S. G. Pavlov, and V. N. Shastin, Appl. Phys. Lett. **72**, 1140 (1998).
[6] A. V. Muravjov, R. C. Strijbos, C. J. Fredricksen, S. H. Withers, W. Trimble, S. G. Pavlov, V. N. Shastin, and R. E. Peale, Appl. Phys. Lett. **74**, 167 (1999).
[7] A. V. Muravjov, S. H. Withers, R. C. Strijbos, S. G. Pavlov, V. N. Shastin, and R. E. Peale, Appl. Phys. Lett. **75**, 2882 (1999).
[8] A. V. Muravjov, R. C. Strijbos, C. J. Fredricksen, H. Weidner, W. Trimble, S. H. Withers, S. G. Pavlov, V. N. Shastin, and R. E. Peale, Appl. Phys. Lett. **73**, 3037 (1998).
[9] A. V. Murav'ev, I. M. Nefedov, S. G. Pavlov, and V. N. Shastin, Kvantovaya Elektron. (Moscow) **20**, 142 (1993) [Sov. J. Quantum Electron. **23**, 119 (1993)].
[10] A. V. Muravjov, S. H. Withers, H. Weidner, R. C. Strijbos, S. G. Pavlov, V. N. Shastin, and R. E. Peale, Appl. Phys. Lett. **76**, 1996 (2000).
[11] E. W. Nelson, A. V. Muravjov, S. G. Pavlov, V. N. Shastin, and R. E. Peale, Infrared Phys. Technol. **42**, 107 (2001).
[12] S. Komiyama, H. Morita, and I. Hosako, Jpn. J. Appl. Phys., Part 1 **32**, 4987 (1993).
[13] T. W. Du Bosq, R. E. Peale, E. W. Nelson, A. V. Muravjov, C. J. Fredricksen, N. Tache, and D. B. Tanner, J. Appl. Phys. **94**, 5474 (2003).
[14] T. W. Du Bosq, R. E. Peale, E. W. Nelson, A. V. Muravjov, D. A. Walters, G. Subramanian, K. B. Sundaram, and C. J. Fredricksen, Opt. Laser Technol. (to be published).
[15] E. Bründermann, A. M. Linhart, H. P. Röser, O. D. Dubon, W. L. Hansen, and E. E. Haller, Appl. Phys. Lett. **68**, 1359 (1996).
[16] R. C. Strijbos, *Hole Transport Effects in p-Ge Lasers*, Ph.D. dissertation, Technische Universiteit Delft, The Netherlands, 1997.
[17] A. V. Murav'ev, I. M. Nefedov, Yu. N. Nozdrin, and V. N. Shastin, Fiz. Tekh. Poluprovodn. (S.-Peterburg) **23**, 1728 (1989) [Semiconductors **23**, 1071 (1989)].
[18] Yu. A. Mityagin, V. N. Murzin, and S. A. Stoklitsky, Opt. Quantum Electron. **23**, S287 (1991).
[19] E. Bründermann, A. M. Linhart, L. Reichertz, H. P. Röser, O. D. Dubon, W. L. Hansen, G. Sirmain, and E. E. Haller, Appl. Phys. Lett. **68**, 3075 (1996).
[20] N. Hiromoto, I. Hosako, and M. Fujiwara, Appl. Phys. Lett. **74**, 3432 (1999).
[21] S. V. Demihovsky, A. V. Murav'ev, S. G. Pavlov, and V. N. Shastin, Semicond. Sci. Technol. **7**, B622 (1991).
[22] Yu. A. Mityagin, V. N. Murzin, O. N. Stepanov, and S. A. Stoklitsky, Semicond. Sci. Technol. **7**, B641 (1991).
[23] A. V. Murav'ev, Yu. N. Nozdrin, S. A. Pavlov, and V. N. Shastin, Pis'ma Zh. Tekh. Fiz. **13**, 65 (1987) [Sov. Tech. Phys. Lett. **13**, 26 (1987)].
[24] F. Keilmann, V. N. Shastin, and R. Till, Appl. Phys. Lett. **58**, 2205 (1991).
[25] F. Keilmann and H. Zuckermann, Opt. Commun. **109**, 296 (1994).
[26] M. V. Dolguikh, A. V. Muravjov, and R. E. Peale, Proc. SPIE **5365**, 184 (2004).
[27] C. J. Fredricksen, E. W. Nelson, A. V. Muravjov, and R. E. Peale, Infrared Phys. Technol. **44**, 79 (2003).
[28] S. Shlimak, Phys. Solid State **41**, 716 (1999).
[29] H. Fritzsche and M. Cuevas, Phys. Rev. **119**, 1238 (1960).
[30] K. M. Itoh, E. E. Haller, W. L. Hansen, J. W. Beeman, J. W. Farmer, A. Rudnev, A. Tikhomirov, and V. I. Ozhogin, Appl. Phys. Lett. **64**, 2121 (1994).
[31] E. W. Nelson, E. S. Flitsiyan, A. V. Muravjov, M. V. Dolguikh, R. E. Peale, S. H. Kleckley, W. G. Vernetson, and V. Z. Tsipin, Proc. SPIE **4993**, 10 (2003).
[32] E. W. Nelson, M. V. Dolguikh, E. S. Flitsiyan, A. V. Muravjov, R. E. Peale, S. H. Kleckley, W. G. Vernetson, and V. Z. Tsipin, Proc. SPIE **5087**, 133 (2003).
[33] E. Bründermann (private communication).
[34] L. E. Vorobjev, S. N. Danilov, and V. I. Stafeev, Opt. Quantum Electron. **23**, S195 (1991).
[35] M. B. Prince, Phys. Rev. **92**, 681 (1953).
[36] F. J. Morin and J. P. Maita, Phys. Rev. **94**, 1525 (1954).
[37] E. W. Nelson, Ph.D. Dissertation, University of Central Florida, Orlando FL, 2003.